3-13-2001

Universality Classes of Self-Avoiding Fixed-Connectivity Membranes

Mark Bowick
Department of Physics, Syracuse University, Syracuse, NY

Angelo Cacciuto
Syracuse University

Gudmar Thorleifsson
deCODE Genetics, Lynghalsi

Alex Travesset
Syracuse University

Universality Classes of Self-Avoiding Fixed-Connectivity Membranes

Mark J. Bowick[(1)*], Angelo Cacciuto[(1)‡]
Gudmar Thorleifsson[(2)†] and Alex Travesset[(1)§]

[1]Physics Department, Syracuse University,
Syracuse, NY 13244-1130, USA
[2] deCODE Genetics, Lynghalsi 1, IS-110
Reykjavik, Iceland

Abstract

We present an analysis of extensive large-scale Monte Carlo simulations of self-avoiding *fixed-connectivity* membranes for sizes (number of faces) ranging from 512 to 17672 (triangular) plaquettes. Self-avoidance is implemented via *impenetrable* plaquettes. We simulate the impenetrable plaquette model in both three and four bulk dimensions. In both cases we find the membrane to be *flat* for all temperatures: the size exponent in three dimensions is $\nu = 0.95(5)$ (Hausdorff dimension $d_H = 2.1(1)$). The single flat phase appears, furthermore, to be equivalent to the large bending rigidity phase of *non-self-avoiding* fixed-connectivity membranes – the roughness exponent in three dimensions is $\xi = 0.63(4)$. This suggests that there is a unique universality class for flat fixed-connectivity membranes without attractive interactions. Finally we address some theoretical and experimental implications of our work.

*bowick@physics.syr.edu ‡cacciuto@physics.syr.edu
†thorleif@decode.is §alex@physics.syr.edu

1 Introduction

There are many different physical systems occurring in nature that we can theoretically model as *fixed-connectivity* membranes [1, 2, 3, 4]. A fixed-connectivity membrane is a *two-dimensional* mesh, in a d-dimensional bulk space, whose nodes have a time-independent coordination number. In other words the connectivity of the mesh is fixed in time, although there may be some spatial variation, provided the resultant density of defects (dislocations and disclinations) is small enough to preserve, at zero temperature, the quasi-long-range translational order and true long-range bond orientational order characteristic of two-dimensional crystals [5, 6, 7]. The statistical mechanics of such membranes is a two-dimensional version of the already rich statistical mechanics of essentially one-dimensional polymers [8, 9, 3, 4]. The physical bulk dimensions are $d = 2$, corresponding to monolayers or planar crystals, and $d = 3$, corresponding to membranes. The intrinsic importance of this universality class of membranes is enhanced by the wealth of examples provided by the natural world. These include the spectrin/actin cytoskeleton of mammalian red blood cells [10], polymerized amphiphilic bilayers and monolayers [11], polymerized polymer sheets [12], graphitic oxides [13, 14, 15], metal dichalcogenides [16] and large sheet molecules of glassy B_2O_3 [17]. Experimental measurements of the physical properties of these real-world fixed-connectivity membranes can be compared with the results of theoretical models and numerical simulations. This is an active area of research on the experimental side, with the exciting possibility of novel membranes such as two-dimensional cross-linked DNA networks. A systematic and deep understanding of this field is also essential in developing theoretical models of more complex systems, such as the complete cell membrane, in which a cytoskeleton (a fixed-connectivity membrane) is coupled to an amphiphilic bilayer (itself a liquid-like membrane) by protein junctional complexes [18].

The statistical mechanics of *phantom* (self-intersecting) fixed-connectivity membranes is governed by the competition between the *elastic* energy of stretching and shearing deformations and the *bending* energy of shape fluctuations. This competition leads to a scale-dependent running of the bending rigidity and elastic moduli of the Hamiltonian in the presence of thermal fluctuations, with the membrane stiffening under bending and softening under elastic deformations as the length scale grows. The upshot is a low-temperature ordered phase, characterized by an infinite persistence length and a spontaneous orientation of the membrane in the bulk space, and a high-

temperature *crumpled* phase with a finite persistence length and no preferred orientation in the bulk. The remarkable ordered phase, conventionally known by the inapt name *flat* phase, is one of the key reasons for the excitement in this field. Furthermore the global flat and crumpled phases are separated by a continuous *crumpling* transition associated with an ultraviolet-stable fixed point in the renormalization group flow of the bending rigidity. The crumpling transition is another exciting feature of the physics of phantom fixed-connectivity membranes.

Realistic fixed-connectivity membranes are, however, *self-avoiding* (SA) in the sense that self-intersections will be energetically costly. This self-avoiding, or excluded-volume, interaction arises at the microscopic (nanometer) scale from the short range repulsion between any two monomers in the membrane. Study of this self-avoiding interaction has proven remarkably difficult. Analytical studies (see [3] and [4] for recent reviews) are ambiguous in that there is a variety of results for, say, critical exponents. This has made it difficult to know the precise nature of the global phase diagram and to reliably predict the key critical exponents. Numerical results using the balls and springs (BS) model, to be discussed in more detail below, clearly indicate that any degree of self-avoidance flattens the membrane at all temperatures. In other words the crumpled phase is unstable to the inclusion of self-avoidance. With its loss goes also the crumpling transition. It has been argued, however, that the loss of the crumpled phase is a result of the particular *discretization* of self-avoidance within the BS models, rather than a universal feature of self-avoidance itself [19]. In particular distant-neighbor interactions due to the excluded volume of the balls can induce an effective bending rigidity for these models even with vanishing bare bending rigidity [19]. Subsequent careful studies of BS models support the claim that the crumpled phase is lost (see Sec.2). More light can be cast on the problem, however, by exploring an alternative discretization of a SA fixed-connectivity membrane known as the *impenetrable plaquette* (IP) model. This will be the focus of the work presented in the rest of the paper. Impenetrable plaquette models have the advantage that the described membrane is extremely flexible in that individual plaquettes are completely free to fold on themselves. As a result they do not suffer from induced bending rigidity. The organization of the paper is as follows. In the next section we provide a quick overview of the BS models for completeness. In Sect.3 we introduce and discuss the impenetrable plaquette model studied in this paper. In Sect.4 we describe the details of the algorithms used to numerically simulate the model. A

complete presentation of our results is given in Sect.5 for the cases of bulk dimensions $d = 3$ and $d = 4$. Finally we summarize in Sect.6 and discuss the implications of our work for the experimentalist and outline some promising future directions.

2 Self-avoidance: Numerical Studies

The self-avoidance interaction at long distances (typically of the order of a micron) may be modeled by generalizing the Edwards model of a self-avoiding polymer [20] to objects with internal dimension D:

$$\mathcal{H}_{SA} = \frac{b}{2} \int d^D\mathbf{x} d^D\mathbf{x}' \delta^d(\vec{r}(\mathbf{x}) - \vec{r}(\mathbf{x}')) \ , \tag{1}$$

where b is the dimensionless parameter governing the strength of self-avoidance.

This implementation of self-avoidance captures the underlying universal physics for a broad class of microscopic potentials describing the interactions between the monomers of the membrane at the nanometer scale.

The most direct discretization of fixed-connectivity membranes including self-avoidance is a network of N monomers arranged in a triangular array. Nearest neighbors interact with a potential [21]

$$V_{NN}(\vec{r}) = \begin{cases} 0 & \text{for } |\vec{r}| < \rho \\ \infty & \text{for } |\vec{r}| > \rho \end{cases} \ , \tag{2}$$

or a smoother variation. The tether length ρ is of the order of a few lattice spacings. The self-avoidance, or excluded volume, is introduced as a repulsive hard sphere potential, now acting between any two monomers in the membrane, instead of only nearest neighbors. A typical hard sphere repulsive potential is

$$V_{Exc}(\vec{r}) = \begin{cases} \infty & \text{for } |\vec{r}| < \sigma \\ 0 & \text{for } |\vec{r}| > \sigma \end{cases} \ , \tag{3}$$

where σ is the range of the potential, and $\sigma < \rho$. Once again some smoother versions of this potential, continuous at $|\vec{r}| = \sigma$, have also been adopted. This model may be pictured as a network of springs, defined by the nearest-neighbor potential Eq.2, with self-avoidance enforced by the finite radius σ of the balls (Eq.3) and we will often refer to it as the BS (balls and springs) model.

There is conclusive evidence that the phase diagram of the three-dimensional BS model consists of a single flat phase – the crumpled phase being lost entirely [19,22-28]. A detailed review may be found in [3].

Simulations for bulk dimension above three have also been performed [22, 23] and provide clear evidence that the membrane remains flat in three and four dimensions and undergoes a crumpling transition for bulk dimension $d \geq 5$, implying that the lowest dimension, d_c, in which a crumpled phase exists is five ($d_c = 5$).

It has been argued [19] that the absence of a crumpled phase is due to induced bending rigidity from distant (next-to-nearest neighbor) excluded volume effects. This may place the self-avoiding membrane in the flat phase of the phantom membrane phase diagram (see [3] and references therein), in which case one expects the flat phase of the self-avoiding and phantom membranes to be equivalent. If this is indeed the case, sufficiently weak excluded volume interactions should induce a bending rigidity below the critical crumpling transition coupling, leading to a crumpled self-avoiding phase. No conclusive evidence for this self-avoiding crumpled phase has been reported. This suggests that flatness is an inevitable consequence of self-avoidance combined with the fixed-connectivity (integrity) of the membrane. This picture would be much more convincing if it could be shown to apply to other models of self-avoiding fixed-connectivity membranes.

An alternative model of self-avoidance is provided by the impenetrable plaquette model (IP), first simulated in [24, 25]. These authors found a size exponent corresponding to a crumpled phase and compatible with the standard Flory estimate. A subsequent simulation [26] of a variation of the IP model, contradicted the results of [24, 25] by claiming a flat phase, but found a fractal size exponent, from the finite-size scaling of the radius of gyration, of $\nu = 0.87$ (no errors quoted). This corresponds to a Hausdorff dimension $d_H = 2.3$, which is neither Flory nor flat. In contrast, the analysis of the orientationally-averaged structure function in [26] gives a different fractal value $\nu = 0.75 (d_H = 2.67)$ (no errors quoted). In short the status of the phase diagram for the IP model is currently murky, in contrast to the clear picture emerging from the BS models outlined earlier.

Motivated by this unsatisfactory state of affairs we turn now to an analysis of our particular realization of the IP model.

3 The Impenetrable Plaquette Model

3.1 GENERAL CASE

The general discretized energy for a flexible phantom triangular fixed-connectivity membrane with bending rigidity κ is given by [27, 3]

$$\mathcal{H}_{\rm ph} = \frac{\epsilon}{2} \sum_{<a,b>} \left(|\vec{r}_a - \vec{r}_b| - 1 \right)^2 + \kappa \sum_{<\alpha,\beta>} (1 - \vec{n}_\alpha \cdot \vec{n}_\beta) \ , \tag{4}$$

where the elastic term is summed over distinct nearest-neighbor pairs of monomers a and b and the bending term is summed over all pairs of adjacent triangular plaquettes α and β. In the free energy $F_{\rm ph}$ the parameter ϵ is a discrete version of the elastic moduli (the Lamé coefficients) of the continuum elastic theory [27], $\vec{n}_\gamma$ is the unit normal to the plaquette γ and the mean lattice spacing has been rescaled to unity without loss of generality. For SA membranes $F_{\rm ph}$ must be supplemented by a discretized version of the Edwards self-avoidance term introduced in Eq.1.

Without self-avoidance the phantom membrane is crumpled for all temperatures above the critical crumpling temperature – the microscopic bending rigidity is scale-dependent and driven to zero at long wavelength by thermal fluctuations. In this regime only the elastic term is relevant in Eq.4. Under the rescaling of the bulk coordinate $\vec{r} \to \vec{r}/\sqrt{\beta}$ we find

$$\beta\mathcal{H} = \frac{\epsilon}{2} \sum_{<a,b>} \left(|\vec{r}_a - \vec{r}_b|^2 - 2\sqrt{\beta}|\vec{r}_a - \vec{r}_b| + \text{const.} \right) \ , \tag{5}$$

which reduces to the pure Gaussian model in the high-temperature limit $\beta \to 0$.

Suppose we can establish that self-avoidance flattens the Gaussian model, which corresponds to the elastic term in Eq.4 with vanishing mean lattice spacing. Then clearly the SA model Eq.4, together with self-avoidance, will also be flat at all temperatures.

3.2 DISCRETIZATION

The continuum Edwards model Eq.1, for membranes ($D = 2$), is then

$$\mathcal{H} = \int d^2\mathbf{x} \partial_\alpha \vec{r} \partial^\alpha \vec{r} + \frac{b}{2} \int d^2\mathbf{x} d^2\mathbf{x}' \delta^d(\vec{r}(\mathbf{x}) - \vec{r}(\mathbf{x}')) \ , \tag{6}$$

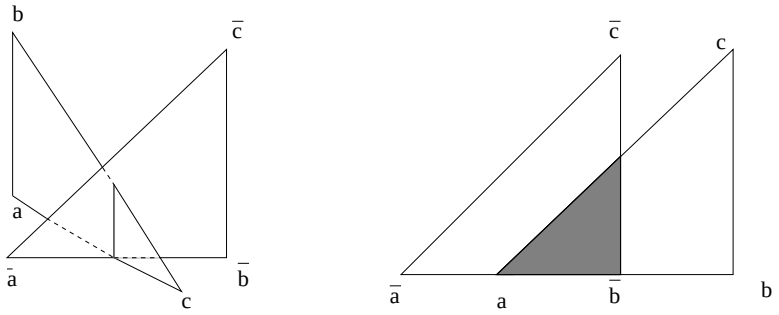

Figure 1: Two intersecting triangles in three dimensions. In the first case the self-avoiding energy is finite, while in the second it is infinite.

where d is the bulk dimension.

Let's apply this to piecewise flat surfaces defined by N vertices $(\vec{r}_a)_{1\leq a\leq N}$, with all vertices, except those at the boundary, being six-coordinated. Any point on the surface is within a triangle defined by its three vertices $\{\vec{r}_a, \vec{r}_b, \vec{r}_c\}$, and may be parametrized as

$$\vec{r}(\alpha,\beta) = \alpha\vec{r}_a + \beta\vec{r}_b + (1-\alpha-\beta)\vec{r}_c \ , \tag{7}$$

where $\alpha \geq 0$, $\beta \geq 0$ and $\alpha + \beta \leq 1$.

The first term in Eq.6 is easily discretized as the Gaussian term previously discussed

$$\int d^2\mathbf{x}\partial_\alpha\vec{r}\partial^\alpha\vec{r} = \frac{1}{2}\sum_{<a,b>}(\vec{r}_a - \vec{r}_b)\cdot(\vec{r}_a - \vec{r}_b) \ , \tag{8}$$

whereas for the self-avoiding interaction we have

$$\begin{aligned}\int d^2\mathbf{x}d^2\mathbf{x}'\delta^d(\vec{r}(\mathbf{x}) - \vec{r}(\mathbf{x}')) &= \int d^2\mathbf{x}d^2\mathbf{x}'\prod_{\mu=1}^{d}\delta(r^\mu(\mathbf{x}) - r^\mu(\mathbf{x}')) \\ &= \sum_{i\neq j}\int d\alpha_i d\beta_i d\alpha_j d\beta_j \prod_{\mu=1}^{d}\delta(r^\mu(\mathbf{x}) - r^\mu(\mathbf{x}')) \ ,\end{aligned} \tag{9}$$

where the last sum runs over all distinct pairs of triangles i, j. Each term here can be explicitly evaluated for any given pair of triangles. Non self-intersecting pairs do not contribute to the sum while for self-intersecting triangles the result depends on the dimensionality and the precise type of self-intersection:

- $d = 3$: Triangles may self-intersect in two different ways, as shown in Fig.1. In the first case the self-intersection is a line whereas in the second it is a two-dimensional region. One-dimensional self-intersections have a finite energy given by

$$\int d\alpha d\beta d\overline{\alpha} d\overline{\beta}\, \delta^{(3)}\Big(\vec{r}(\alpha,\beta) - \vec{r}(\overline{\alpha},\overline{\beta})\Big) \propto s \ , \tag{10}$$

  where s is the intersection length. Two-dimensional self-intersections, however, have infinite energies (see Fig.1).

- $d = 4$: The integral is finite if triangles self-intersect in a point but infinite if they intersect in a line or a surface.

- $d \geq 5$ The integral is infinite whenever there is self-intersection.

The model we treat is an open triangular network containing N vertices with free boundary conditions. The energy is

$$\mathcal{H} = \frac{1}{2} \sum_{<ab>} |\vec{r}_a - \vec{r}_b|^2 \ , \tag{11}$$

provided the triangles defining the surface do not intersect anywhere. If two triangles do intersect the configuration is strictly forbidden (its energy is infinite). This discretization corresponds to tuning the self-avoiding coupling in Eq.6 to infinity ($b = \infty$). It may be worthwhile to consider a weaker version of self-avoidance, corresponding to a finite value of b, in which some degree of self-intersection is permissible. This will not be treated in this paper since the computational cost rises significantly and we do not expect the critical behavior to be sensitive to the precise value of b.

We adopted three distinct geometries, each depicted in Fig.2, in our simulations. The 3d simulations employed mostly the c geometry, but the other two geometries were explored as a test of universality. The 4d simulations used the hexagonal geometry a.

The square geometries b and c, with L vertices on a side, have a total number of nodes $N = L^2$. The hexagonal geometry a, with L links on each of the six sides, has a total number of nodes

$$N = 3L^2 + 3L + 1 \ . \tag{12}$$

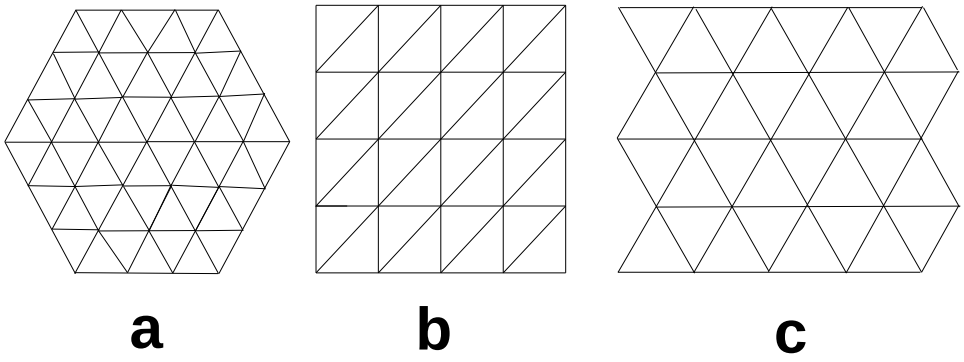

Figure 2: The three lattice geometries adopted in our membrane simulations, where $L = 3$ for **a** and $L = 5$ for **b** and **c**.

3.3 OBSERVABLES and MEASUREMENTS

A comprehensive understanding of the *shape* of a fluctuating membrane may be obtained from a careful analysis of the shape tensor[1] [19, 28, 29],

$$S_{\alpha\beta} = \frac{1}{2N^2}\sum_{k=1}^{N}\sum_{l=1}^{N}(r_{\alpha k} - r_{\alpha l})(r_{\beta k} - r_{\beta l}) = \frac{1}{N}\sum_{k=1}^{N} r_{\alpha k} r_{\beta k} - \frac{1}{N^2}\sum_{k=1}^{N} r_{\alpha k}\sum_{l=1}^{N} r_{\beta l}\ , \tag{13}$$

where the indices k, l run over the lattice. The trace of $S_{\alpha\beta}$ is the squared radius of gyration R_G^2

$$R_G^2 = \mathrm{Tr}\, S_{\alpha\beta}\,. \tag{14}$$

The growth of the radius of gyration with internal system size L determines the Hausdorff dimension d_H, or equivalently, the size exponent $\nu = 2/d_H$, via $R_G \sim L^\nu$. Diagonalizing the (symmetric) shape tensor and performing a statistical average over independent configurations defines d shape exponents β_α via the finite-size scaling of its eigenvalues λ_α

$$\langle \lambda_\alpha \rangle \sim N^{\beta_\alpha}\ , \tag{15}$$

with $\alpha = 1, \cdots, d$. In a crumpled (isotropic) phase all d exponents are equal and given by ν (i.e. $\beta_\alpha = \nu$ for all α). In a flat phase, on the other hand, $\beta_\alpha = 1$ for the two in-plane eigen-directions (say $\alpha = 1, 2$) and the remaining

[1]The shape tensor is obtained from the standard moment of inertia tensor by subtracting out the isotropic contribution and is sometimes also mistakenly called the moment of inertia tensor in the literature.

shape exponents describe the root-mean-square height ($\vec{h}$) fluctuations. For $d = 3$, to be specific, β_3 is the standard roughness exponent ζ ($< h^2 > \sim L^{2\zeta}$) [19, 30].

Further important information on the conformation of the membrane is provided by the structure function, defined as

$$S(\vec{q}) = \frac{1}{N^2} \sum_{a,b} \left\langle e^{i\vec{q}\cdot(\vec{r}_a - \vec{r}_b)} \right\rangle , \tag{16}$$

where $\vec{q}$ is an arbitrary wavevector. In particular the scaling properties of the structure function for wavevectors parallel to the eigenvectors of the shape tensor will allow us to determine the key shape exponents of the model.

4 Simulation Methods

Simulations of self-avoiding membranes are hampered both by long autocorrelation times in updating the embedding coordinates and by the non-locality of the self-avoidance constraint. These two factors combined have effectively prevented simulations of large enough SA fixed-connectivity membranes for a reliable determination of their scaling properties. There has been some recent progress though in overcoming both these problems.

Improved methods for updating the embedding $\{\vec{r}(\mathbf{x})\}$ have been applied in simulations of a *non-SA* (phantom) fixed-connectivity membranes. In [31] three different methods were compared:

- A standard Metropolis updating scheme.
- Hybrid over-relaxation: make a quadratic approximation to the action[2], then apply over-relaxation followed by a Metropolis accept/reject test.
- Unigrid algorithm: update the membrane recursively on all length scales by dividing the lattice into sub-lattices of different sizes and apply a Metropolis algorithm to a collective update of those parts.

The performance of each of these methods – the CPU-cost per independent configuration (T_{CPU}) – is compared in Fig.3. This figure is based on

[2]Note that over-relaxation is exact for vanishing bending rigidity since the action is quadratic.

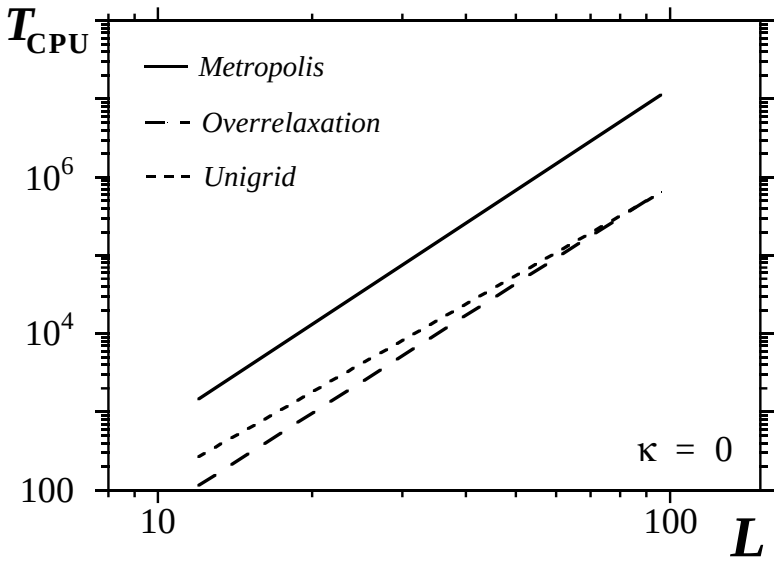

Figure 3: The performance of three different methods for updating the embedding of an isotropic phantom fixed-connectivity membrane.

the values presented in [31]. For the membrane sizes typically used in Monte Carlo simulations, $L < 100$, both the hybrid over-relaxation and the unigrid algorithm reduced the cost ten-fold compared to a simple Metropolis algorithm. Only the unigrid algorithm, however, reduces the dynamical exponent z, which measures the volume scaling of the CPU-cost ($T_{\mathrm{CPU}} \sim L^z$) from $z = 4$ to $z \approx 3.8$.

The superior over-relaxation and unigrid algorithms are both easily adapted to simulations of SA fixed-connectivity membranes. The real CPU-cost in self-avoiding simulations, on the other hand, is the non-locality of the updating. Implementing SA as impenetrable plaquettes requires a check verifying that the proposed update of the embedding does not lead to intersecting triangles. In addition to being non-local, pairwise intersection-checking is very time-consuming. It is, however, possible to reduce this CPU-cost by a clever implementation of the SA check. We have compared three such implementations:

A A comprehensive check; explicitly verifying that no updated triangle intersects any other triangle in the lattice by comparing all relevant pairs of triangles.

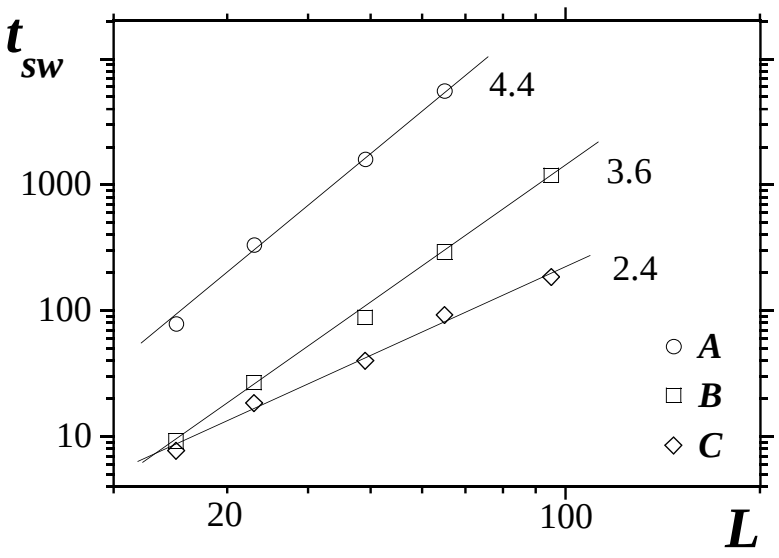

Figure 4: The CPU-times for updating a SA fixed-connectivity membrane ($d = 3$) using hybrid over-relaxation with three different methods of checking for self-intersection. For each method an estimate of the computational-cost exponent is included.

B Inscribe each triangle in a *minimal* sphere in the embedding space. This has the advantage that pairs of triangles whose spheres do not overlap are not compared, and overlapping are quickly identified.

C Inscribe regions (sub-lattices) of the membrane of different sizes in a minimal sphere and apply method **B** *recursively* to regions of decreasing size. In this way large portions of the membrane are quickly eliminated from the checking procedure.

For simplicity we use these methods in combination with a hybrid over-relaxation algorithm as it updates the membrane locally. Although it is not a priori clear that the unigrid algorithm, which performs a non-local update, should perform any worse than the over-relaxation applied to SA-membranes, it would be more complicated to implement the above methods.

In Fig.4 we compare the CPU-times for one sweep of hybrid over-relaxation for each of these methods. Methods **B** and **C** reduce the overall CPU-time substantially and, more importantly, both improve the volume scaling of the CPU-cost: from $t_{\rm sw} \sim L^{4.4}$ for method **A** to $t_{\rm sw} \sim L^{2.4}$ for method **C**.

N	τ_{R_G}	IND CONF	N	τ_{R_G}	IND CONF
289	2000	2500	2401	20000	150
625	7000	1300	4225	40000	80
1089	12000	350	9025	71000	30

Table 1: Number of independent configurations (IND CONF) for each volume for $d = 3$.

The simulations were done on several different machines; Pentium II (250 MHz), IBM SP2 (160 MHz) and a DEC ALPHA workstation cluster. The total computational cost of the three-dimensional simulation was equivalent to 150,000 SP2 hours while that for the four-dimensional simulation was 60,000 SP2 hours. The total number of sweeps depends on the volume and configurations are stored after a certain fixed number of sweeps. The total number of independent configurations for each volume and dimension can be read off from Tables 1[3] and 2.

We next address the quality of our data. Given an observable O we measure, after thermalization, the autocorrelation time τ_O

$$\tau_O(T) = \frac{1}{2} + \sum_{t=1}^{T} \rho_O(t) \ , \tag{17}$$

where the normalized autocorrelation function $\rho_O(t)$ is given by

$$\rho_O(t) = \frac{(\frac{1}{M-t}\sum_{i=1}^{M-t} O_i O_{i+t} - \langle O \rangle^2)}{(\langle O^2 \rangle - \langle O \rangle^2)} \ . \tag{18}$$

and T is a cutoff generally taken to be the largest value for which ρ does not become negative [32].

In Tables 1 ($d = 3$) and 2($d = 4$) we list autocorrelation times for the shape tensor, one of the slowest observables of the membrane. There is a striking dependence on volume.

A cross-check of statistical independence may be performed by studying the error bars as a function of bin size. It is well known that the error bar for any observable O scales as a function of the bin size as

$$\sigma_O(n_b)/\sigma_O(1) \sim \sqrt{(2\tau_O + 1)} \tag{19}$$

[3]Note that the autocorrelation times in this table do not give the correct finite-size scaling exponent z because the larger volumes were simulated with a more effective algorithm than the smaller volumes.

N	MC ($\times 10^5$)	TH($\times 10^4$)	τ_{R_G}	IND CONF
61	5.5	5	8.2(6)	67073
127	8.0	10	26.0(9)	30769
217	8.0	10	80(10)	10000
331	13.0	30	210(35)	6190
469	12.0	20	400(40)	3000
817	12.0	32	1000(100)	1200
1261	16.0	40	3400(700)	470

Table 2: Number of Monte Carlo sweeps performed for each volume for bulk dimension $d = 4$, where a Monte Carlo sweep is defined as a combined Metropolis and over-relaxation sweep. The number of thermalization sweeps is also listed, together with the autocorrelation times of the shape tensor and the net number of independent configurations.

where the bin size n_b must be big enough for bins to be statistically independent. To further ensure the statistical independence of our data, we verified this dependence in all our measurements. As a concrete example, we plot in Fig.5 the error bar for S_{22} as a function of the bin size. A clear plateau is observed corresponding to an error bar $\sigma = 0.011$. We also find $\sigma(1) = 0.0025$. ¿From Eq.19 we get $\tau_{eff} = 9.2$. Since measurements were taken every 20 sweeps, we have $\tau_{R_G} = 20$ and $\tau_{eff} = 184$, in good agreement with the result given in Table 2.

In summary we believe that we have done the requisite checks to ensure the statistical independence of our data and we move on to a discussion of results.

5 Measurement of Observables

5.1 BULK DIMENSION $d = 3$

The first observables we analyze are the eigenvalues of the shape tensor Eq.13. In Fig.6 we plot the distribution of the shape tensor eigenvalues for $L = 33$ ($N = 1089$) and $L = 65$ ($N = 4225$). There is a clear first peak, which we identify with height fluctuations, and a second peak which we identify with size fluctuations. The slight double well structure of the second peak is a reflection of the asymmetry of the adopted geometry, as illustrated in

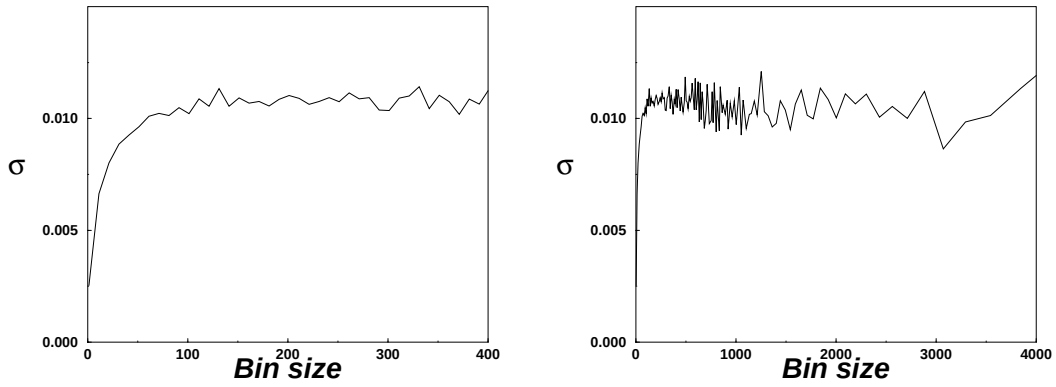

Figure 5: Plot of a typical error bar as a function of the bin size. The left figure magnifies the small size bins of the right one. This particular plot correspond to the observable S_{22} at volume $N = 331$ ($d = 4$). Measurements were taken every 20 sweeps.

Fig.2. The overall double peak distribution of eigenvalues corresponds to an anisotropic surface resulting from rotational symmetry breaking and is the first signal of an orientationally ordered (*flat*) phase. Indeed, the distribution of eigenvalues found here is similar to that found in the flat phase of a phantom fixed-connectivity membrane [29].

We next determine the three exponents β_α from the power law scaling given in Eq.15. The results are shown in Tables 3 and 4. The column corresponding to Fit1 is a direct fit to the power law, including all volumes, whereas Fit2 excludes volumes $N < 625$. To investigate the role played by the boundary (we have free boundary conditions), we also perform fits excluding nodes near the boundary. Excluding nodes beyond $0.9 \times L$ from the center, we perform a full fit (Fit3) or a fit removing sizes $N < 625$ (Fit4). We also report similar fits (Fit5 and Fit6) excluding nodes beyond $0.8 \times L$ from the center. It is evident that the membrane does not exhibit strong edge fluctuations.

This analysis gives a size exponent ν near one and a roughness exponent $\zeta = 0.65(1)$. Our results show a slight dependence on the volumes included in the fit, indicating that sub-leading corrections are not negligible. We repeated the fits using two different parametrizations of the sub-leading corrections. This is shown in Table 4. This improved the quality of the fits

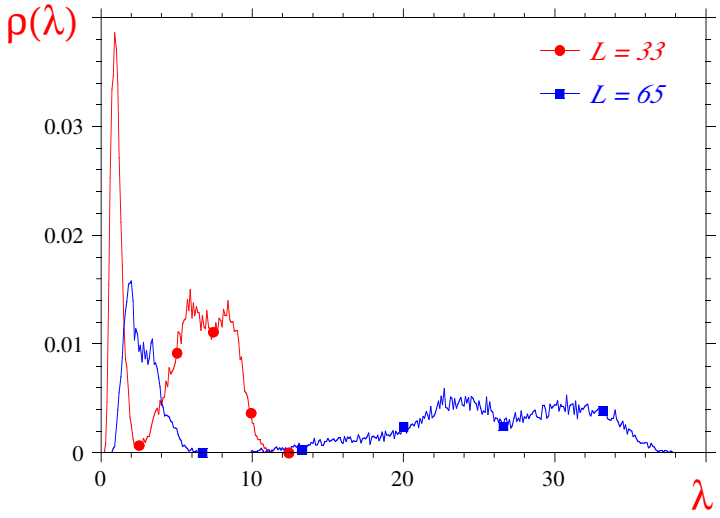

Figure 6: Distribution of the eigenvalues of the shape tensor for volumes $N = 1089$ and $N = 4225$ ($d = 3$).

considerably. The size exponent ν moves towards one and the roughness exponent ζ decreases slightly.

Further progress requires study of the structure function, Eq.16. In Fig.7 we plot the structure function along the directions of the largest eigenvalue for different lattice sizes. For small momentum the structure function is monotonically decreasing. For q sufficiently large, however, a series of peaks appear.

¿From the small-q region we can extract the critical exponents ν and ζ. To do so we plot the structure function along the directions corresponding

	Fit1	Fit2	Fit3	Fit4	Fit5	Fit6
ν	0.945(14)	0.959(13)	0.938(13)	0.948(11)	0.918(14)	0.944(13)
ζ	0.655(22)	0.660(33)	0.649(19)	0.655(30)	0.642(16)	0.652(23)

Table 3: Results of the various fits to a simple power law, as described in the text, for the size exponent ν and the roughness exponent ζ ($d = 3$).

fit	ν	χ^2	ζ	χ^2
$aN^\beta + b$	0.945(14)	5.7	0.655(22)	0.994
$aN^\beta + b\log(N)$	0.959(15)	5.3	0.63(1)	5.9

Table 4: Comparison of the size and roughness exponents with two distinct functional forms of sub-leading corrections ($d = 3$). The whole lattice is included in these fits.

to the largest and smallest eigenvalues, respectively, as a function of the scaling variables qL^ν and qL^ζ. Collapse to a single scaling curve is excellent for $\nu = 0.95(5)$ and $\zeta = 0.63(4)$ as illustrated in Figs.8 ($\nu = 0.95$) and 9 ($\zeta = 0.63$) [4]

The analysis of the structure function for larger values of q is also revealing. The picture emerging so far is that a SA fixed-connectivity membrane of linear size L is rough at short distances, of the order of $L_{\rm rough}$, but globally flat. The structure function must exhibit, in this case, peaks at

$$\vec{q}^{\,L}_{(l_1,l_2)} = \frac{\pi}{L/L_{\rm rough}}(l_1\vec{G}_1 + l_2\vec{G}_2)\ ,\ l_1, l_2 = 1, \cdots \tag{20}$$

where $\vec{G}_{1,2}$ are the standard reciprocal vectors for a triangular lattice and the factor π, as opposed to 2π, is a consequence of free rather than periodic boundary conditions. To test Eq.20 we plot in Fig.10 the first (denoted by $n = 1$) and second (denoted by $n = 2$) peaks of the structure function versus $1/L$. There is clearly a very good fit. Furthermore Eq.20 implies that the ratio of wavevectors $q^L_{n=2}/q^L_{n=1} = \sqrt{3}$, which is indeed the case: from the fit we find

$$\frac{b_2}{b_1} = \frac{46}{26} = 1.77 \approx 1.73 = \sqrt{3}\ , \tag{21}$$

where b_n is the slope of the fit (see Fig.10). From Eq.20 we can also extract $L_{\rm rough}$:

$$L_{\rm rough} \approx 8\ . \tag{22}$$

This result clearly indicates that one must work with membranes of linear size L much larger than 8 to effectively eliminate finite-size effects.

Note that the peaks are damped in intensity with increasing n (see Fig.7). This may be attributed to the membrane having an effective thickness, as given by the roughness exponent.

[4]The quoted errors for these scaling exponents are rather insensitive to the precise statistical method by which the quality of the scaling collapse is assessed.

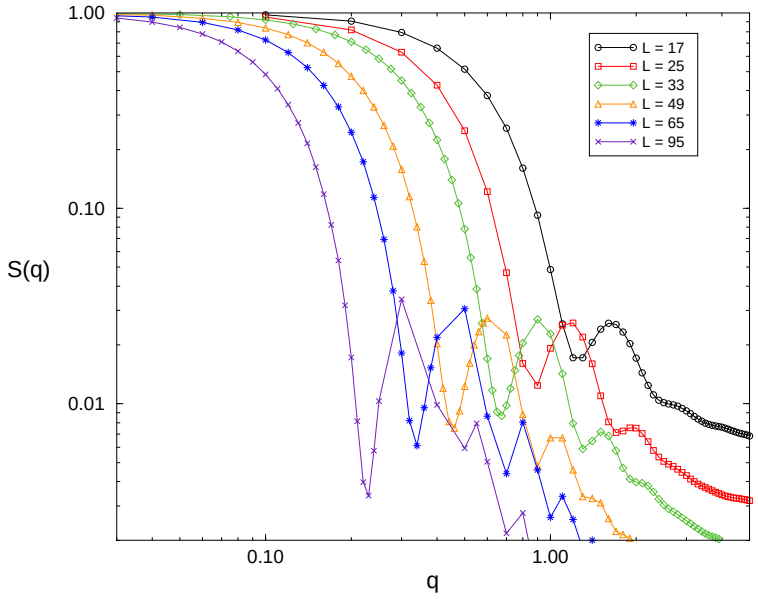

Figure 7: Log-Log plot of the structure functions along the direction of the maximum eigenvalue of the shape tensor as a function of the wave vector q ($d = 3$).

The previous analysis convincingly establishes that the membrane is flat. Further evidence is provided by visualizing typical snapshots of membranes after thermalization. This is shown in Fig.11, where one sees that the membrane is rough at short distances ($L_{\rm rough} \approx 8$ by inspection) but flat on large scales – certainly "a picture is worth more than thousands of numbers." In contrast, a snapshot of a thermalized configuration, with self-avoidance switched off ($b = 0$), is shown in Fig.12. The dramatic effect of self-avoidance is striking. As a final check we performed several simulations with a folded initial state and observed the subsequent unfolding to the flat phase.

5.2 BULK DIMENSION $d = 4$

We start by examining the shape eigenvalues Eq.13. In Fig.13 we plot the distribution of eigenvalues for different volumes. It is clear from the two-peak structure that a crumpled phase can be ruled out. The first peak is associated with height fluctuations and the second with size fluctuations. These plots are in qualitative agreement with those obtained for $d = 3$.

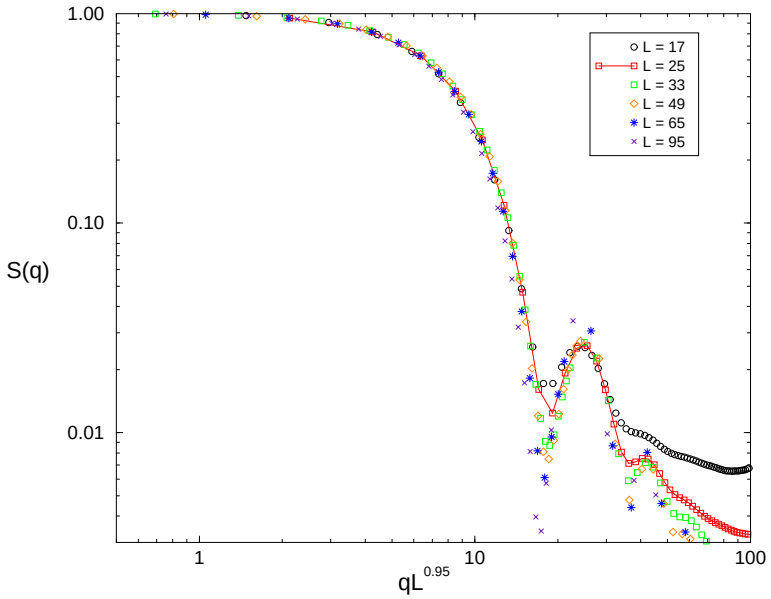

Figure 8: Log-Log plot of the structure function along the direction of the maximum eigenvalue of the shape tensor, as a function of the scaling variable, for each volume simulated ($d = 3$).

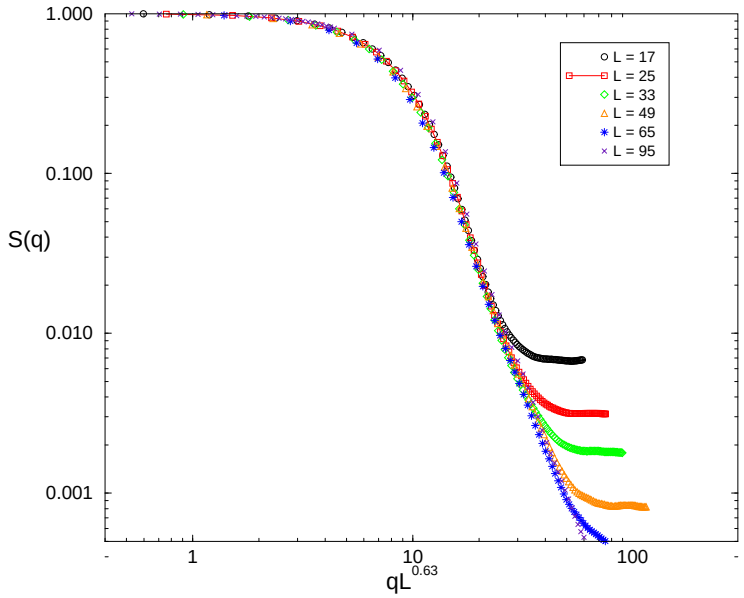

Figure 9: Log-Log plot of the structure function along the direction normal to the preferred plane of the membrane, as a function of the scaling variable, for each volume simulated ($d = 3$).

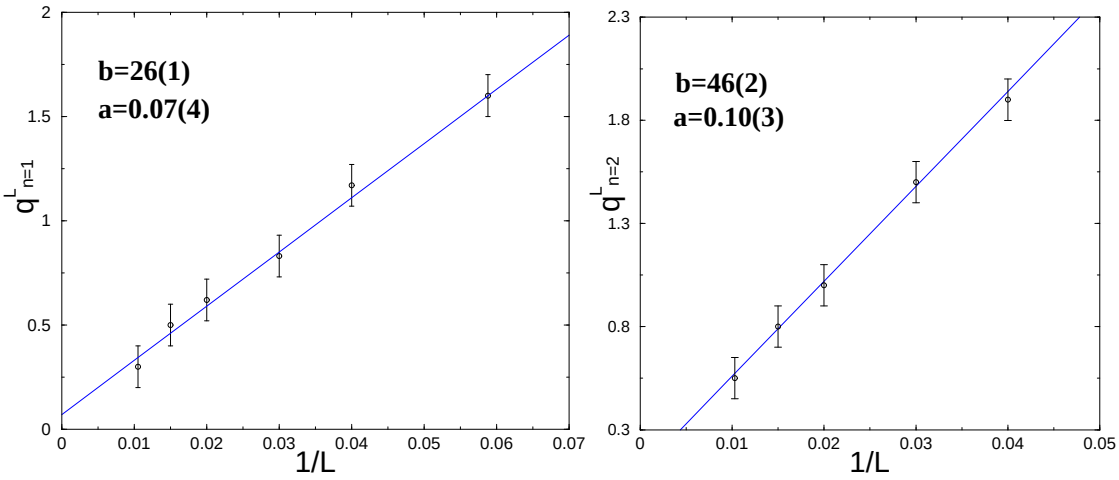

Figure 10: Fits of the peaks of the structure function to the form $q_n^L = a + b_n/L$ $(d = 3)$.

The expectation values of the eigenvalues are plotted as a function of volume in Fig.14. Both λ_1 and λ_2 increase rapidly with volume, while λ_3 and λ_4 grow slowly.

To compute the exponents β_α, we need to fit the data to the functional form in Eq.15, which has three free parameters.

Finite size effects are significant for the range of volumes we analyzed ($N = 127$ to 1261). To evaluate the importance of sub-leading corrections to scaling, we once again fit the data to two distinct functional forms. The results are shown in Tables 5 and 6. The size exponent spans the range

$$\nu = 0.82(4) - 0.90(1) \ , \tag{23}$$

Although sub-leading corrections significantly affect the extracted scaling behavior, it is clear that the size exponent ν is tending to 1. To substantiate this result requires extensive simulations of larger volumes.

In a flat phase, the scaling of the third and fourth eigenvalue is associated with the roughness exponent. The roughness exponent falls in the range

$$\zeta = 0.65(1) - 0.79(1) \ , \tag{24}$$

where again, the errors ignore systematic effects. The roughness exponent is large, so it implies that the membrane, despite being flat (or almost flat)

Figure 11: A snapshot of a thermalized *self-avoiding* configuration for volume $N = 9025$. The membrane is flat over long length scales but rough on short scales ($d = 3$).

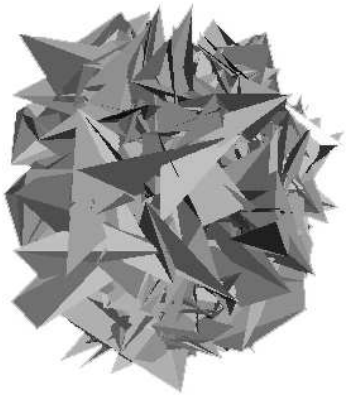

Figure 12: A snapshot of a thermalized configuration ($d = 3$) for a *phantom* membrane ($b = 0$), with vanishing bending rigidity, for comparison with Fig.11 ($N = 4225$).

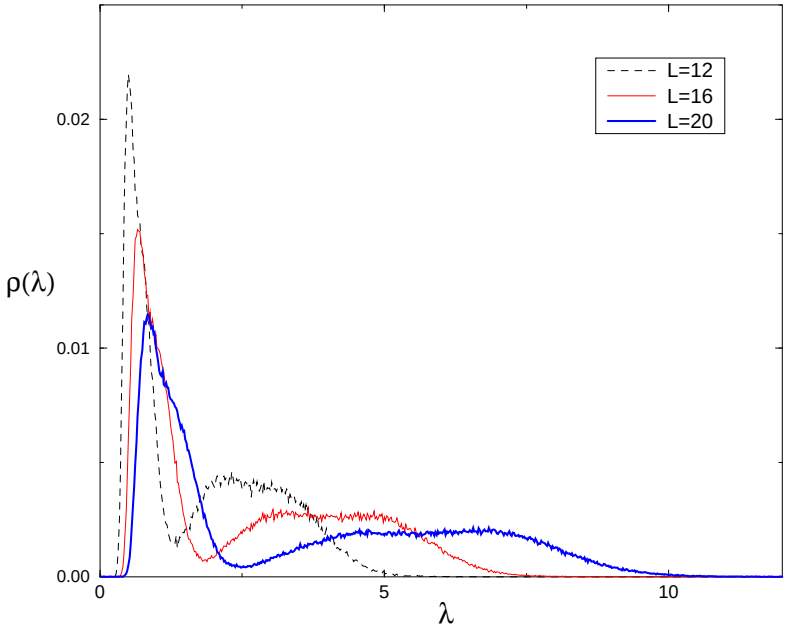

Figure 13: Distribution of eigenvalues for three different volumes $N = 331$, $N = 817$ and $N = 1261$ (d=4).

overall, is very rough. For completeness, we quote the roughness exponent associated with the smallest eigenvalue; it is $\zeta_u = 0.62(7) - 0.74(2)$. It is somewhat smaller than Eq.24 but compatible with it. Whether these two exponents are the same is something we cannot establish, and larger volume sizes are clearly called for.

The other observable we use to study the properties of the membrane is the structure function, defined in Eq.16. As noted earlier, the scaling of the structure function along the direction defined by the largest eigenvalue is directly related to the size exponent. The strategy is to match the structure function as a function of the scaled variable qL^{ν}, where ν is the size exponent. The result of the matching is

$$\nu = 0.9(1) \ , \tag{25}$$

where the error bar needs further explanation. The matching of the structure

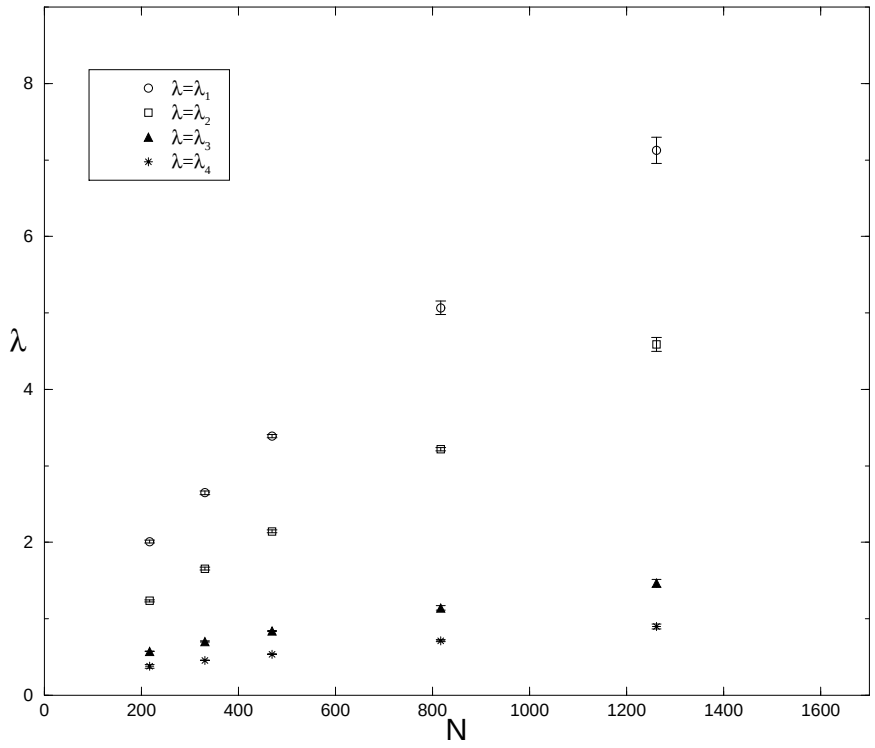

Figure 14: Plot of the eigenvalues as a function of the volume (d=4).

function for small values of q is acceptable for values $\nu \geq 0.8$. Near $\nu = 0.8$ the range of q for which matching is found is somewhat small. This range increases with ν, but if ν is chosen too large (say, $\nu > 1$), the small-q matching deteriorates and is poor. We note that although the matching for $\nu = 1$ is still very good, the best overall value for ν is $\nu = 0.9$. The error bar quoted in Eq. 25 is a conservative estimate embracing the range of acceptable ν.

We also computed evaluated the structure function along the directions of the third and fourth eigenvalue of the shape tensor. This yields a roughness exponent (see Fig.16)

$$\zeta = 0.60(7) \ , \tag{26}$$

in good agreement with the estimates given in Tables 5 and 6. The error bar is a rough estimate indicating the range of exponents that yield acceptable scaling.

The situation for the plaquette model for $d > 4$ is much easier to analyze. Since a two-dimensional surface almost never self-intersects in bulk dimen-

$\mathbf{aN^\beta + b}$	β	a	b	χ^2
λ_1	0.833(8)	0.0172(9)	0.47(2)	0.24
λ_2	0.81(2)	0.013(2)	0.20(3)	0.61
λ_3	0.65(1)	0.0119(9)	0.166(7)	0.22
λ_4	0.620(7)	0.0093(6)	0.112(5)	0.10

Table 5: Fits to finite-size scaling of the form $aN^\beta + b$ for the eigenvalues of the shape tensor ($d = 4$).

$\mathbf{aN^\beta + b\log(N)}$	β	a	b	χ^2
λ_1	0.90(1)	0.010(1)	0.139(6)	0.48
λ_2	0.85(2)	0.0091(2)	0.060(7)	0.60
λ_3	0.788(6)	0.0038(1)	0.0574(1)	0.10
λ_4	0.74(2)	0.0031(4)	0.038(1)	0.22

Table 6: Fits to finite-size scaling of the form $aN^\beta + b\log(N)$ for the eigenvalues of the shape tensor for (d=4).

sions five and above, self-avoidance is irrelevant and the membrane is always crumpled. The radius of gyration for any $d \geq 5$ is given by

$$R_G^2 \sim \log(N) \ , \tag{27}$$

which corresponds to $\nu = 0$, the Gaussian result.

6 Summary and Conclusions

6.1 SUMMARY

In this section we summarize the most important results obtained from the detailed analyses presented earlier. The impenetrable plaquette model for $d = 3$ is flat for all temperatures with critical exponents

$$\nu = 0.97(4) \quad \zeta = 0.63(3) \ , \tag{28}$$

with the error reflecting the range of estimates obtained by the different methods described. The membrane is a flat object at large distances but a very rough one for characteristic linear sizes $L \approx 8$. The values for the critical

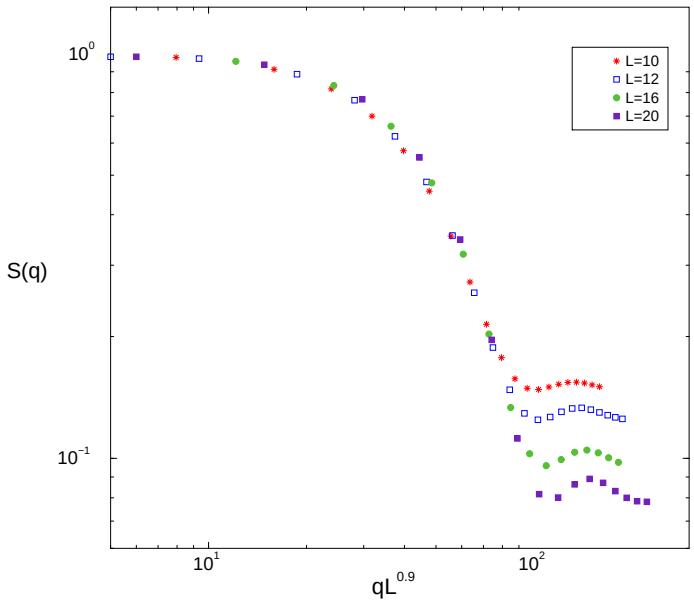

Figure 15: Log-Log plot of the structure function (d=4) along the direction of the maximum eigenvalue of the shape tensor for each volume simulated as a function of the scaling variable qL^{ν} (with $\nu = 0.9$).

exponents are in agreement with the results from BS models (see [3] for a review). The roughness exponent of the flat phase of phantom membranes is given by [29]

$$\zeta = 0.64(2) \ , \tag{29}$$

which agrees very well with the result obtained above. We conclude that there is a single flat phase for fixed-connectivity membranes, describing either a phantom membrane at large bending rigidity or a self-avoiding membrane at any non-negative bending rigidity.

Embedding dimension $d = 4$ has also been studied. Here we find very strong evidence that, for all temperatures, there is once again only a flat phase, with exponents

$$\nu = 0.9(1) \quad \zeta = 0.65(10) \ . \tag{30}$$

In this case the quantitative values for the exponent are not as accurate as we have for $d = 3$ since the lattice volumes considered were not as large and finite size effects give rise to systematic errors. It would be desirable to

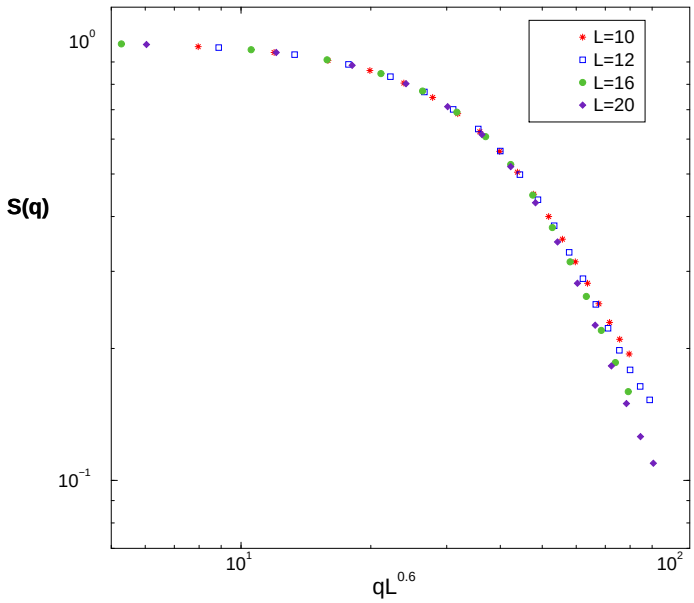

Figure 16: Log-Log plot of the structure function (d=4) along the direction of the minimum eigenvalue of the shape tensor as a function of the scaling variable qL^{ζ} (with $\zeta = 0.6$).

simulate larger volumes to narrow down the exponent $\nu \sim 1$. Gathering all the evidence acquired from the analyses carried out in this paper, however, we find it very unlikely that the size exponent is not one.

6.2 CONCLUSIONS

Our study establishes that the phase diagram of fixed-connectivity membranes is very simple and consists only of a flat phase for both $d = 3$ and $d = 4$, and crumpled phases only for $d > 4$. In order to rigorously compare these theoretical results with experiments, one should consider the effect of topological defects [33], which play an important role in any crystalline phase. One would not expect defects to alter the long-distance properties of the model, however, within the range of temperatures for which the crystalline phase prevails, since the overall integrity (unbroken connectivity) of the mesh combined with self-avoidance are the key triggers of the flat phase. These properties are retained even in the presence of topological defects. This overall picture is consistent with the current experimental situation – no re-

alization of a fixed-connectivity membrane has ever been seen in a crumpled state. The observed flat phases have exponents consistent with the numerical results of this paper.

Analytical results for SA fixed-connectivity membranes are reviewed in [3]. Here we simply note that the ϵ-expansion, at zero bending rigidity, predicts a unique infra-red stable fixed point and no phase transitions, in agreement with our simulations. The current value of the size exponent within the ϵ-expansion, computed to two-loop order in [34, 35] (see [4] for a review), however, definitely seems to be less than one. It would be of great interest to know if the inclusion of higher-orders in the expansion pushes ν towards the flat value of one.

It is also important to remark that the previous results assume repulsive potentials among the monomers. When this restriction is dropped and attractive forces are considered [19], the picture actually changes, and compact phases [36] seem to be possible (see also [37, 38]. This very interesting possibility may naturally occur in some systems, so it will certainly be the subject of subsequent work.

Our results also have implications for other models. It is well known that anisotropic fixed-connectivity membranes possess an intermediate tubular phase [39, 40]. Since the tubular phase is, very roughly speaking, crumpled in one dimension only, it has been argued that it may survive the incorporation of self-avoidance [41, 42, 43]. Anisotropy cannot be readily introduced in our model, since if we tune the self-avoidance coupling to zero, we automatically sit in the crumpled phase where anisotropy is known to be an irrelevant perturbation. Since adding anisotropic extrinsic curvature to the self-avoiding membrane will only flatten the membrane even more, this cannot produce a tubular phase either. One should therefore consider different discretizations for the self-avoiding case than the ones that are suitable for the phantom model discussed in [40].

The understanding of the physical properties of fixed-connectivity membranes are also very important in constructing realistic models of full-fledged cell membranes. The next step in this very exciting goal would be to describe a model of a coupled fluid and fixed-connectivity membrane. Since one can safely assume (provided no attractive forces are present) that the fixed-connectivity membrane is flat, this property alone significantly constrains the different effective theories that need to be considered. This is just one of the many exciting problems that physicists will need to tackle in the near future.

Acknowledgements

We acknowledge fruitful discussions with Mehran Kardar. The work of MB, AC and AT was supported by the U.S. Department of Energy under contract No. DE-FG02-85ER40237. Some computational resources were provided by a grant from NPACI.

References

[1] D. R. Nelson, *The statistical mechanics of membranes and interfaces*, in Nelson et al. [8].

[2] F. David, *Introduction to the statistical mechanics of random surfaces and membranes*, in "Two Dimensional Quantum Gravity and Random Surfaces", Vol. **8** of *Jerusalem Winter School for Theoretical Physics*, D.J. Gross, T. Piran, and S. Weinberg (Eds.) (World Scientific, Singapore, 1992).

[3] M. Bowick and A. Travesset, *The Statistical Mechanics of Membranes*, in "Renormalization Group Theory at the Turn of the Millennium," D. O'Connor and C.R. Stephens (Eds.) Phys. Rep. **344** (2001) 255-310: cond-mat/0002038.

[4] K. J. Wiese, *Polymerized Membranes, a Review*, in Vol. **19** of "Phase Transitions and Critical Phenomena", pp.253-480: C. Domb and J. L. Lebowitz (Eds) (Academic Press, 2001): cond-mat/0001345.

[5] D.R. Nelson and B.I. Halperin, Phys. Rev. **B19** (1979) 2457.

[6] A.P. Young, Phys. Rev. **B19** (1979) 1855.

[7] D. R. Nelson, Phys. Rev. **B18** (1978) 2318.

[8] *Statistical Mechanics of Membranes and Surfaces*, Vol. **5** of "Jerusalem Winter School for Theoretical Physics," D.R. Nelson, T. Piran and S. Weinberg (Eds.) (World Scientific, Singapore, 1989).

[9] S.A. Safran, *Statistical Thermodynamics of Surfaces, Interfaces, and Membranes* (Addison Wesley, Reading, Massachusetts, 1994).

[10] C. F. Schmidt, K. Svoboda, N. Lei, I. B. Petsche, L. E. Berman, C. R. Safinya, and G. S. Grest, *Existence of a flat phase in red cell membrane skeletons*, Science **259** (1993) 952.

[11] J.H. Fendler, Chem. Rev. **87** (1987) 877.

[12] S.I. Stupp, S. Son, H.C. Lin and L.S. Li, Science **259** (1993) 59.

[13] T. Hwa, E. Kokufuta, and T. Tanaka, *Conformation of graphite oxide membranes in solution*, Phys. Rev. **A44** (1991) R2235.

[14] X. Wen, C. W. Garland, T. Hwa, M. Kardar, E. Kokufuta, Y. Li, M. Orkisz and T. Tanaka, Nature **355** (1992) 426.

[15] M.S. Spector, E. Naranjo, S. Chiruvolu and J.A. Zasadzinski, Phys. Rev. Lett. **73** (1994) 2867.

[16] R.R. Chianelli, E.B. Prestridge, T.A. Pecoraro and J.P. DeNeufville, Science **203** (1979) 1105.

[17] M.J.Aziz, E.Nygren, J.F.Hays and D. Turnbull, Jour. Appl. Phys. **57** (1985) 2233.

[18] B. Alberts, D. Bray, J. Lewis, M. Raff, K. Roberts and J. D. Watson, *Molecular Biology Of The Cell* (Third Edition), Garland Publishing, New York, 1994.

[19] F.F. Abraham and D.R. Nelson, *Fluctuations in the flat and collapsed phase of polymerized surfaces*, J. Phys. (France) **51** (1990) 2653.

[20] S.F. Edwards, Proc. R. Soc. London Ser. **A85** (1965) 613.

[21] Y. Kantor, M. Kardar, and D.R. Nelson, *Statistical mechanics of tethered surfaces*, Phys. Rev. Lett. **57** (1986) 791.

[22] G. Grest, J. Phys. I (France) **1** (1991) 1695.

[23] S. J. Barsky and M. Plischke, *Molecular dynamics simulation of tethered membranes in four and five dimensions*, Phys. Rev. **E50** (1994) 3911.

[24] A. Baumgärtner, *Does a polymerized membrane crumple?* J. Phys. I (France) **1** (1991) 1549.

[25] A. Baumgärtner and W. Renz, *Crumpled Self-Avoiding Tethered Surfaces*, Europhys. Lett. **17** (1992) 381.

[26] D.M. Kroll and G. Gompper, *Floppy tethered networks*, J. Phys. (France) **3** (1993) 1131.

[27] H. S. Seung and D. R. Nelson, *Defects in flexible membranes with crystalline order*, Phys. Rev. **A38** (1988) 1005.

[28] Y. Kantor and K. Kremer, *Excluded volume interactions in tethered membranes*, Phys. Rev. **E48** (1993) 2490.

[29] M. J. Bowick, S. M. Catterall, M. Falcioni, G. Thorleifsson and K. N. Anagnostopoulos, *The flat phase of crystalline membranes*, J. Phys. I (France) **6** (1996) 1321: cond-mat/9603157.

[30] F.F. Abraham and D.R. Nelson, *Diffraction from polymerized membranes*, Science **249** (1990) 393.

[31] G. Thorleifsson and M. Falcioni, *Improved algorithms for simulating crystalline membranes*, Computer Phys. Comm. **109** (1998) 161: physics/9709026.

[32] A.D. Sokal, *Monte Carlo Methods in Statistical Mechanics: Foundations and New Algorithms*, Cours de la Troiseme Cycle de la Physique en Suisse Romande, Laussane, June 1989.

[33] D. R. Nelson, *Defects in superfluids, superconductors and membranes*, in "Fluctuating Geometries in Statistical Mechanics and Field Theory," F. David, P. Ginsparg, and J. Zinn-Justin (Eds;) Les Houches Summer School (North-Holland, Amsterdam, 1996): arXiv.org/lh94.

[34] F. David and K. J. Wiese, *Scaling of selfavoiding tethered membranes: 2-loop renormalization group results*, Phys. Rev. Lett. **76** (1996) 4564: cond-mat/960215.

[35] K. J. Wiese and F. David, *New Renormalization Group Results for Scaling of Self-Avoiding Membranes*, Nucl. Phys. **B487** (1997) 529: cond-mat/9608022.

[36] F. F. Abraham and M. Kardar, *Folding and unbinding transitions in tethered membranes*, Science **252** (1991) 419.

[37] D. Liu and M. Plischke, Phys. Rev. **A45** (1992) 7139.

[38] G. S. Grest and I. B. Petsche, Phys. Rev. **E50** (1994) 1737.

[39] L. Radzihovsky and J. Toner, *A New Phase of Tethered Membranes: Tubules*, Phys. Rev. Lett. **75** (1995) 4752: cond-mat/9510172.

[40] M. Bowick, M. Falcioni and G. Thorleifsson, *Numerical Observation of a Tubular Phase in Anisotropic Membranes*, Phys. Rev. Lett. **79** (1997) 885: cond-mat/9705059.

[41] M. Bowick and E. Guitter, *Effects of self-avoidance on the tubular phase of anistropic membranes*, Phys. Rev. **E56** (1997) 7023: cond-mat/9705045.

[42] L. Radzihovsky and J. Toner, *Elasticity, Shape Fluctuations and Phase Transitions in the New Tubule Phase of Anisotropic Tethered Membranes*, Phys. Rev. **E57** (1998) 1832: cond-mat/9708046.

[43] M. Bowick and A. Travesset, *Tubular phase of self-avoiding anisotropic crystalline membranes*, Phys. Rev. **E59** (1999) 5659: cond-mat/9808214.